JBC RESEARCH ARTICLE

14-3-3 interaction with phosphodiesterase 8A sustains PKA signaling and downregulates the MAPK pathway

Received for publication, January 8, 2024 Published, Papers in Press, February 6, 2024,
https://doi.org/10.1016/j.jbc.2024.105725

Soumita Mukherjee[1], Somesh Roy[1], Shruti Mukherjee[2], Amaravadhi Harikishore[3], Anirban Bhunia[2], and Atin K. Mandal[1,*]

From the [1]Department of Biological Sciences, and [2]Department of Chemical Sciences, Bose Institute, Kolkata, India; [3]School of Biological Sciences, Nanyang Technological University, Singapore, Singapore

Reviewed by members of the JBC Editorial Board. Edited by Wolfgang Peti

The cAMP/PKA and mitogen-activated protein kinase (MAPK) signaling cascade control many cellular processes and are highly regulated for optimal cellular responses upon external stimuli. Phosphodiesterase 8A (PDE8A) is an important regulator that inhibits signaling *via* cAMP-dependent PKA by hydrolyzing intracellular cAMP pool. Conversely, PDE8A activates the MAPK pathway by protecting CRAF/Raf1 kinase from PKA-mediated inhibitory phosphorylation at Ser259 residue, a binding site of scaffold protein 14-3-3. It still remains enigmatic as to how the cross-talk involving PDE8A regulation influences cAMP/PKA and MAPK signaling pathways. Here, we report that PDE8A interacts with 14-3-3ζ in both yeast and mammalian system, and this interaction is enhanced upon the activation of PKA, which phosphorylates PDE8A's Ser359 residue. Biophysical characterization of phospho-Ser359 peptide with 14-3-3ζ protein further supports their interaction. Strikingly, 14-3-3ζ reduces the catalytic activity of PDE8A, which upregulates the cAMP/PKA pathway while the MAPK pathway is downregulated. Moreover, 14-3-3ζ in complex with PDE8A and cAMP-bound regulatory subunit of PKA, RIα, delays the deactivation of PKA signaling. Our results define 14-3-3ζ as a molecular switch that operates signaling between cAMP/PKA and MAPK by associating with PDE8A.

Phosphodiesterase(s) (PDEs) are a family of enzymes that regulate cell functions by decreasing the intracellular levels of cAMP and cGMP, both of which are "second messengers" involved in relaying signal received by cell-surface receptor to effector proteins. PDEs inactivate signaling by hydrolyzing cAMP, cGMP, or both generated in response to the activation of a wide range of membrane receptors. Among the 11 families of mammalian PDE identified so far, PDE5, PDE6, and PDE9 are specific for cGMP, whereas PDE4, PDE7, and PDE8 are cAMP-specific, and the rest can hydrolyze both (1, 2). Since inhibition of PDEs elevates cAMP and cGMP levels, there is a surge of interest to generate PDE inhibitors which are used in treating diseases such as asthma, chronic obstructive pulmonary disease, erectile-dysfunction, depression, and hypertension (3–5).

Recent studies establish that scaffold proteins, by protein–protein interaction, play a central role in regulating cAMP-mediated signaling. These scaffold proteins are responsible for the subcellular targeting of some PDEs and co-ordinating cAMP's cellular effects (6, 7). Studies also indicate the creation of nonoverlapping intracellular cAMP compartments where cAMP effectors, PKA, PDEs along with scaffold proteins (such as A-kinase anchoring proteins) form localized signaling complex to manoeuvre the effects of cAMP. For example, the PDE4 family interact with AKAPs, β-arrestins, and receptor for activated PKC that regulate its enzyme activity and subcellular localization (6, 7). Likewise, it was found that PDE3B interacts with phospho-motif binding scaffold protein 14-3-3β in rat adipocytes in response to insulin (8). Further study showed that PDE3B phosphorylation by PKA facilitates its interaction with 14-3-3 and sustains PDE3B catalytic activity by protecting it from phosphatase-mediated deactivation (9). Similarly, PMA-induced phosphorylation of PDE3A at Ser428 residue was found to be necessary for its interaction with 14-3-3 (10).

PDE8A is one of the recently identified PDEs of the PDE8 family, having an N-terminal response regulator receiver and a per–arnt–sim domain (11). It is expressed abundantly in the testis, ovary, small intestine, and colon and is insensitive to most common PDE inhibitors, for example, 3-isobutyl-1-methylxanthine (IBMX). PDE8A regulates critical cellular events such as T-cell adhesion, lymphocyte chemotaxis, steroidogenesis, and excitation-contraction coupling (12–16). Like PDE3B, PDE8A is also phosphorylated by PKA, which boosts its catalytic activity and is a part of the feedback loop that restores basal cAMP levels (17). Interestingly, PDE8A is involved in the cross-talk between mitogen-activated protein kinase (MAPK) and the cAMP/PKA signaling pathway, where it acts as an activator of the MAPK pathway. It binds to CRAF/Raf1 (MAP3K) and generates a localized compartment where PKA-mediated inhibitory phosphorylation on Ser259 residue of CRAF is reduced by local hydrolysis of the cAMP pool (18). But while PDE8A remains tightly bound to CRAF in cells, which might lead to improper MAPK activation, it is unclear how this activation of the MAPK pathway by PDE8A is regulated or controlled (18). PDE8A–CRAF complex has

* For correspondence: Atin K. Mandal, mandalak@jcbose.ac.in.

significant clinical implications because it has been demonstrated that disrupting this complex is a promising therapeutic approach for the treatment of resistant melanoma (19). Intriguingly, Ser259 phosphorylation of CRAF mediated by PKA allows binding of 14-3-3 protein at this site that locks CRAF in an inactive state, leading to inhibition of the MAPK pathway. Therefore, a complex interplay of PDE8A, 14-3-3, and CRAF protein exists in the cellular milieu, which governs cross-talk between cAMP–PKA and MAPK pathway.

Here, we report the interaction of PDE8A with 14-3-3ζ, which modulates the signaling through cAMP/PKA and the MAPK pathway. 14-3-3ζ binds to the phosphorylated Ser359 residue of PDE8A with its phosphorylation-binding pocket consisting of positively charged Arg residues (R56 and R60). Interestingly, this interaction takes place in the absence of CRAF protein, a common binding partner of both 14-3-3 and PDE8A, indicating a direct role of 14-3-3 on PDE8A. Biophysical studies further confirm the interaction of purified 14-3-3ξ protein with phosphopeptide synthesized around the Ser359 residue of PDE8A. Our result suggests that 14-3-3ζ acts as an intrinsic inhibitor of the PDE activity of PDE8A, which sustains the cAMP–PKA pathway, while impairing the phosphorylation of ERK1/2 and MAPK pathway. Therefore, 14-3-3ζ functions as a switch by regulating the activity of PDE8A.

Results

PDE8A interacts with 14-3-3 protein

PDE8A mediated upregulation of CRAF activity by reducing inhibitory Ser259 phosphorylation, as well as the potential therapeutic benefit of blocking the PDE8–CRAF complex in resistant melanoma, prompted us to seek potential PDE8A regulators (18, 19). Since 14-3-3 binds to the phosphorylated Ser259 residue to retain CRAF in an inactive state, it is possible that 14-3-3 controls PDE8A. So, we investigated whether human 14-3-3 protein interacts with PDE8A. Overexpressed FLAG-PDE8A in HEK293T cells was immunoprecipitated with anti-FLAG antibody, and the 14-3-3 association was checked with anti-14-3-3 pan antibody (Fig. 1*A*). We observed a band corresponding to endogenous 14-3-3 protein in association with PDE8A (Fig. 1*A*, lane 2), which enhanced substantially upon cross-linking with 1% formaldehyde (Fig. 1*A*, lanes 3 and 4). This result suggests that PDE8A may interact with 14-3-3 protein, as previously shown for PDE3 (9, 10). Mammalian cells have seven isoforms of 14-3-3 proteins, whereas yeast has only two, BMH1 and BMH2. It has previously been shown that mammalian 14-3-3 protein can substitute yeast BMH1 and BMH2 proteins (20). To simplify the complexity and confirm the interaction between PDE8A and 14-3-3, we utilized yeast system to see if two yeast 14-3-3 isoforms, BMH1 and BMH2, can also interact with human PDE8A. To test this, hemagglutinin (HA)-tagged BMH1/BMH2 were immunoprecipitated from *bmh1Δ* and *bmh2Δ* cells coexpressing Myc-tagged PDE8A, respectively. Confirming our data from mammalian cells, both the yeast isoforms BMH1 and BMH2 interacted strongly with Myc-PDE8A (Fig. 1*B*, lanes 2 and 4). Next, we looked into which of the seven 14-3-3 isoforms found in mammalian cells has preferential binding to PDE8A. Five isoforms of human 14-3-3 (ζ, β, η, ε, and σ) were selected, and their association was checked by coexpressing them with human MYC-PDE8A in HEK293T cells. Immunoprecipitation (IP) data showed that 14-3-3ζ interacted strongly than others (Fig. 1*C*, lane 3), indicating that 14-3-3ζ is the preferential isoform for human PDE8A. Interaction studies with overexpressed 14-3-3ζ and Myc-PDE8A in HEK293T cells also showed similar results (Fig. 1*D*, lane 4). Additionally, the interaction between endogenous PDE8A and 14-3-3ζ was also detected in cancer cell lines HCT116 (colon) and MCF7 (breast) (Fig. 1, *E* and *F*). It is important to note that 14-3-3ζ preferentially forms dimer (Fig. S1) but monomeric form exists with distinct physiological functions (21). Any preference of PDE8A binding to the monomeric or dimeric 14-3-3ζ was tested by using a mutant 14-3-3ξ construct (14-3-3ζm) with three amino acid substitutions (^{12}LAE^{14} to ^{12}QQR^{14}) at the dimer interface, resulting in its monomerization (22). The result showed that monomeric 14-3-3ξ (14-3-3ζm) can interact with PDE8A comparable to WT 14-3-3ζ (Fig. 1*G*, lanes 2 and 3).

As stated earlier, CRAF kinase is a shared binding partner of PDE8A and 14-3-3. As a consequence, the observed association of human PDE8A with 14-3-3ζ could be direct or indirect *via* CRAF kinase. To address this issue, the interaction of these proteins was examined in yeast system lacking CRAF kinase. In yeast cells, Myc-PDE8A and His-14-3-3ζ were expressed and the interaction was checked by pulling 14-3-3ζ with an anti-His antibody. PDE8A binds to 14-3-3ζ even in the absence of CRAF, indicating a direct association (Fig. 2*A*, lane 2). Additionally, we have studied the interaction with a phosphomimetic 14-3-3ζ mutant (T232E) in HEK293T cells, which was earlier reported to have reduced association with CRAF (23). PDE8A binds equally with both WT and T232E 14-3-3, implying a direct interaction (Fig. 2*B*). Finally, PDE8A–14-3-3ζ interaction was seen in CRAF knockout (CRAF$^{-/-}$) HEK293T cells confirming their direct association (Fig. 2*C*). Overall, our data demonstrates that PDE8A and 14-3-3ξ interact in the cellular environment.

PKA mediates PDE8A–14-3-3ζ interaction

PKA, PKC, and PKB are known to regulate the functions of PDE by phosphorylating different sites; for example, PKA phosphorylates PDE1A, PDE3, PDE4, PDE5A, PDE10A2; PKB phosphorylate PDE3; and PKC phosphorylates PDE3B (1). Some phosphorylation modulates the PDE activity by inhibiting or activating PDE activity, changing cellular localization or interaction with adapter proteins. We predicted that protein kinase (PKA/PKC/PKB) would be involved in sustaining the PDE8A–14-3-3 interaction since 14-3-3 proteins bind to phosphorylated residues on the target protein. A previous study has shown that PKA activates PDE8A by phosphorylating its Ser359 residue (17). In order to investigate if PKA is involved in the PDE8A–14-3-3 interaction, HEK293T cells were treated independently with forskolin and H-89, which are activator and inhibitor of PKA, respectively. We found an

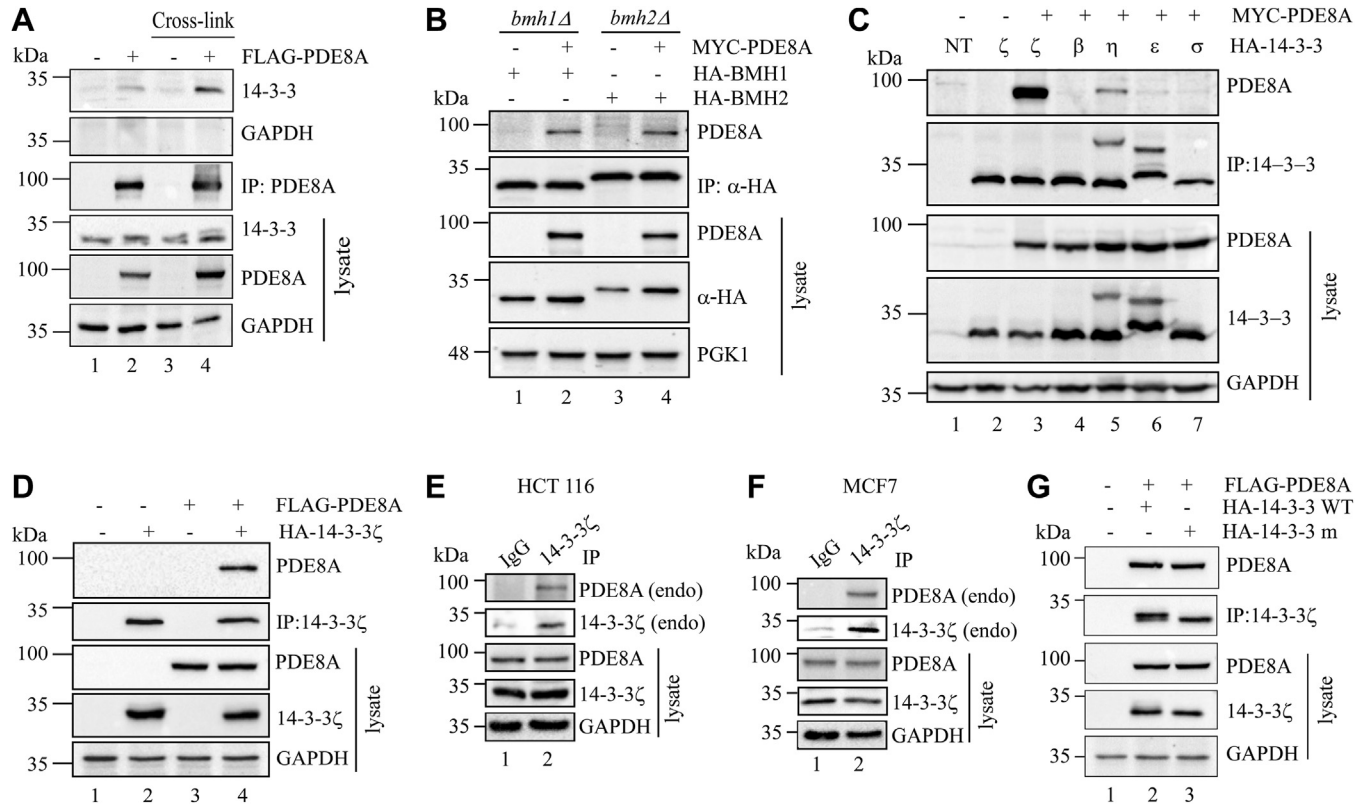

Figure 1. PDE8A interacts with 14-3-3. *A*, the association of PDE8A with endogenous 14-3-3 was checked by immunoprecipitating overexpressed FLAG-PDE8A with anti-FLAG antibody and then immunoblotting with anti-14-3-3 pan antibody. *B*, yeast isoforms of the 14-3-3 protein *BMH1* and *BHM2* were cloned into yeast vector with HA-tag and coexpressed with MYC-PDE8A in *bmh1Δ* and *bmh2Δ* yeast cells, respectively. Anti-HA antibody was used to immunoprecipitated BMH1 and BMH2, and anti-MYC antibody was utilized for testing PDE8A interaction. *C*, the interaction of five mammalian HA-tagged 14-3-3 isoforms [zeta (ζ), beta (β), eta (η), epsilon (ε), and sigma (σ)] with PDE8A was studied by coexpression with MYC-PDE8A. 14-3-3 was pulled by anti-HA antibody and PDE8A was detected with anti-Myc antibody. *D*, PDE8A and 14-3-3 interaction was validated by overexpression of both in HEK293T cells, followed by immunoprecipitation and detection using anti-HA and anti-FLAG antibodies. *E* and *F*, 14-3-3ζ antibody was used to pull endogenous 14-3-3ζ from HCT116 (*E*) and MCF7 (*F*) cell lines. Subsequently, the association of endogenous PDE8A with 14-3-3ζ pulled from HCT116 and MCF7 was detected using antibody specific to PDE8A. *G*, PDE8A binding to dimeric and monomeric 14-3-3ζm (^{12}LAE^{14} to ^{12}QQR^{14}) was examined after coexpression of both constructs in HEK293T cells, followed by pulldown of 14-3-3with anti-HA antibody. Anti-FLAG antibody was used to detect PDE8A. GAPDH or PGK1 were used as loading control in mammalian and yeast cells, respectively. Representative blots of three independent experiments are shown (n = 3). HA, hemagglutinin; NT, nontransfected cell control; PDE8A, phosphodiesterase 8A.

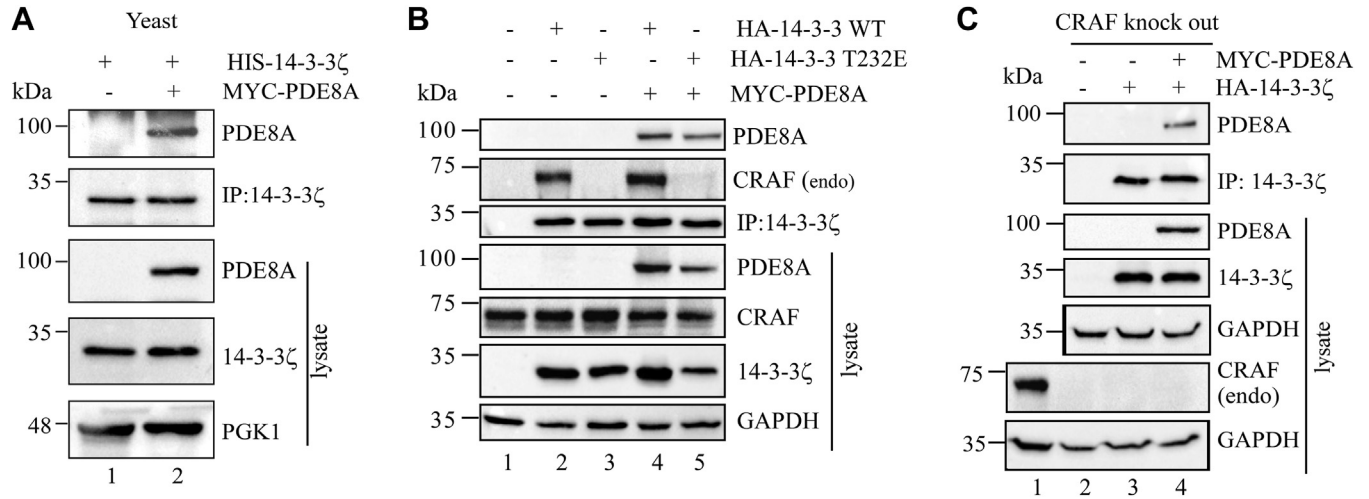

Figure 2. PDE8A interacts with 14-3-3ζ in the absence of CRAF. *A*, MYC-PDE8A and HIS-14-3-3ζ was overexpressed in BY4741 yeast cells, and 14-3-3ζ was pulled with anti-His antibody and immunoblotted with anti-Myc antibody to see the association with PDE8A. *B*, MYC-PDE8A was coexpressed with HA-tagged WT and T232E 14-3-3ζ in HEK293T cells. 14-3-3ζ was immunoprecipitated with anti-HA antibody and the binding of PDE8A and CRAF were confirmed with anti-Myc and endogenous anti-CRAF antibody, respectively. *C*, interaction of MYC-PDE8A and HA-14-3-3ζ was checked in CRAF knockout ($CRAF^{-/-}$) HEK293T cell to determine if PDE8A can interact with 14-3-3ζ in the absence of CRAF. Anti-HA antibody was used to immunoprecipitate 14-3-3ζ and coimmunoprecipitation was confirmed with anti-Myc antibody. An endogenous anti-CRAF antibody was used to validate CRAF knockdown in whole-cell lysate. GAPDH or PGK1 served as loading control for whole-cell lysate in mammalian and yeast cells, respectively. HA, hemagglutinin; PDE8A, phosphodiesterase 8A.

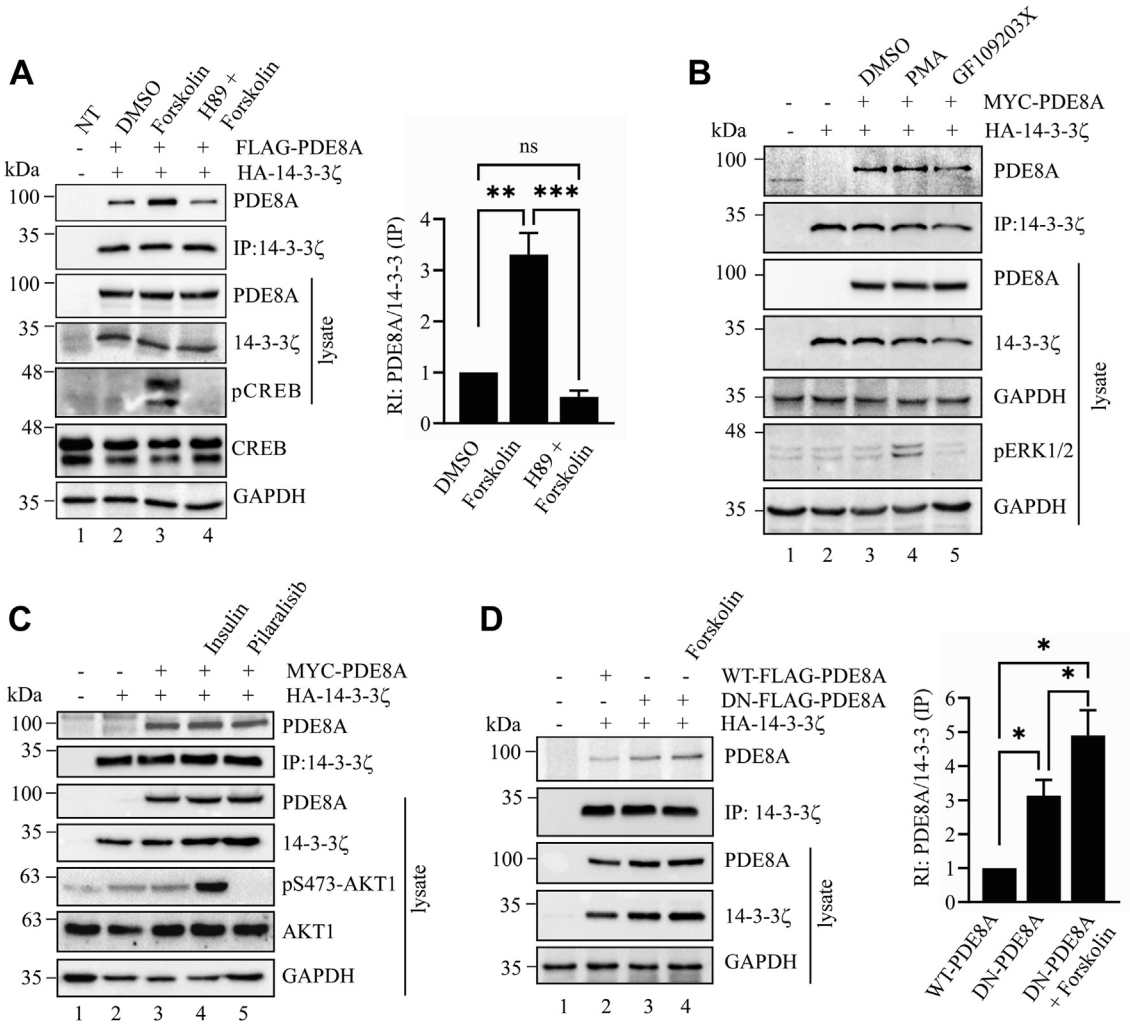

Figure 3. PKA modulates interaction of PDE8A and 14-3-3ζ. FLAG or MYC-tagged PDE8A were cotransfected with HA-14-3-3ζ in HEK293T cells. The effect of protein kinases in the binding of PDE8A-14-3-3 was monitored upon treating the cells with activator/inhibitor of PKA (forskolin/H89), PKC (PMA/GF109203X), and PI3K (insulin/pilaralisib). Cells were treated with serum-free media containing forskolin (100 μM, 15 min) or H89 (100 μM, 15 min pre-treatment), followed by forskolin (100 μM, 15 min) (*A*); and PMA (1 μM, 15 min) or GF109203X (1 μM, 15 min) (*B*); insulin (200 μM, 30 min) or pilaralisib (100 μM, 30 min) (*C*). *D*, WT or DN-PDE8A was cotransfected with HA-14-3-3ζ with or without treatment with forskolin (100 μM, 15 min). 14-3-3ζ was immunoprecipitated with anti-HA antibody and coimmunoprecipitation of PDE8A was checked with anti-FLAG/Myc antibody as indicated. GAPDH served as loading control. *A* and *D*, relative intensity (RI) of MYC- or FLAG-PDE8A coimmunoprecipated with respect to 14-3-3ζ immunoprecipitated from each sample was quantified and represented in adjacent graph (mean ± SEM). Each experiment was repeated at least thrice. *$p < 0.05$, **$p < 0.01$, and ***$p < 0.001$ respectively, significance was analyzed using one-way ANOVA. HA, hemagglutinin; NT, nontransfected cell control; PDE8A, phosphodiesterase 8A.

increased association of PDE8A-14-3-3ζ when PKA was activated by forskolin, on the contrary, this association decreased in the case of H89 (Fig. 3*A*, lanes 3 and 4). In comparison, no change of interaction was observed when cells were treated with PKC activator (PMA) and inhibitor (GX109203X) (Fig. 3*B*, lanes 4 and 5). Similarly, the interaction between PDE8A and 14-3-3ζ remained unchanged when the PKB/AKT pathway was activated with insulin, activator of PI3K or inhibited with pilaralisib, an inhibitor of PI3K (Fig. 3*C*, lanes 4 and 5). These results indicate that phosphorylation of PDE8A by PKA drives the interaction with 14-3-3ζ.

To further corroborate this finding, we used D726A PDE8A mutant or DN-PDE8A, a dominant negative catalytically dead form known to be rapidly phosphorylated by PKA following forskolin treatment (17). Since this catalytically dead form of PDE8A is more phosphorylated than WT PDE8A, it interacted with 14-3-3ζ more than the WT, and this interaction was increased further upon treatment with forskolin (Fig. 3*D*, lanes 2, 3, and 4). These results strongly imply that PKA phosphorylation is required for PDE8A to interact with 14-3-3ζ.

14-3-3 interacts with Ser359 residue of PDE8A

Bioinformatics analysis by SCANSITE 4.0 (24) suggests that PDE8A has three putative 14-3-3 mode 1 interaction motifs (RXXpSXX) similar to PDE3B at residues Ser 359, 380, and 386 (Fig. S2). To identify the 14-3-3 interaction site on PDE8A, these serine residues were mutated individually to Ala (S359A, S380A, S386A), and their interaction was checked with HA-14-3-3ζ in HEK293T cells. In agreement with the fact that Ser359 is phosphorylated by PKA (17), S359A substitution lost the ability to interact with 14-3-3ξ protein; however,

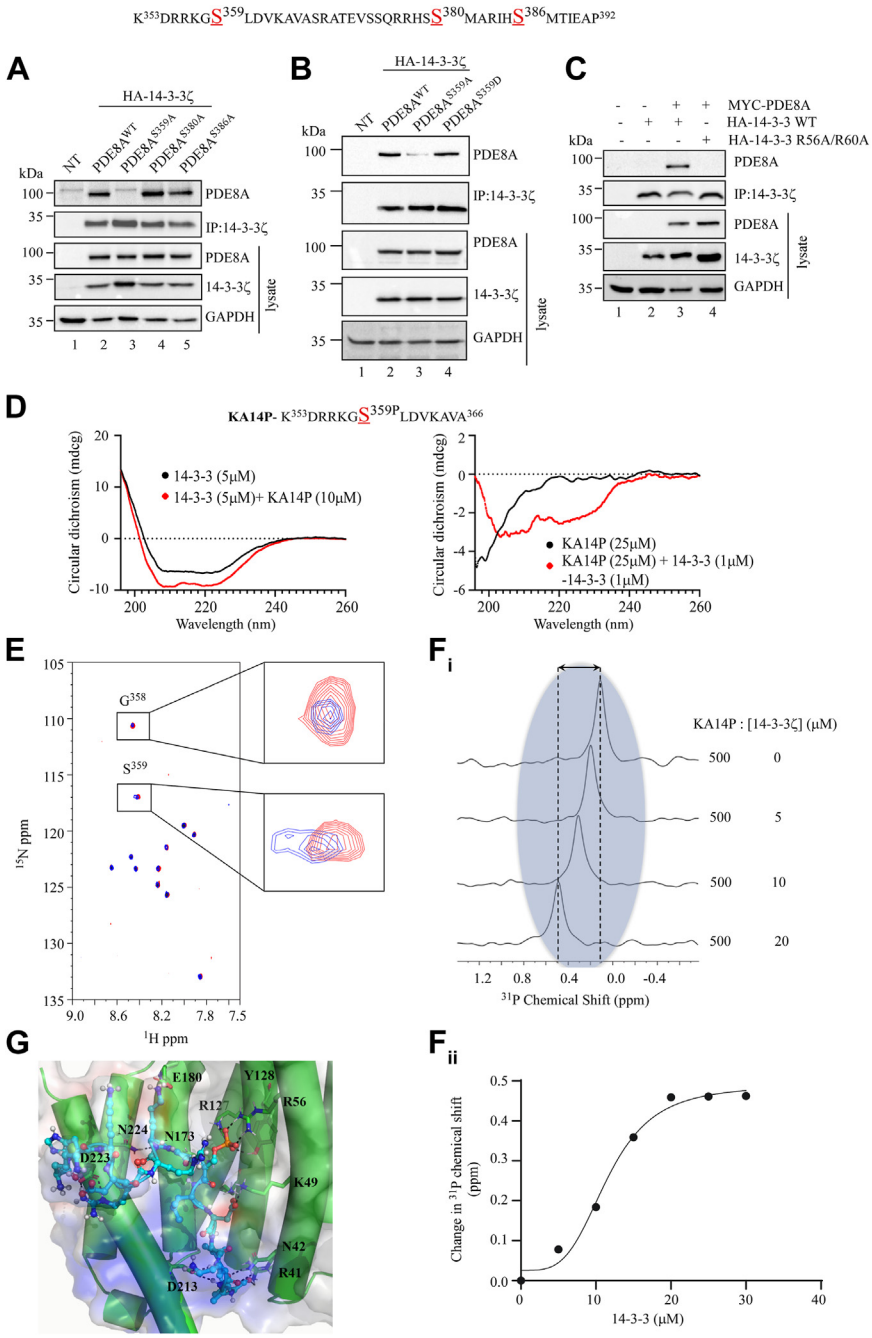

Figure 4. Phosphorylation dependent binding of PDE8A with 14-3-3ζ. *A* and *B*, the putative 14-3-3 interaction sites of PDE8A S356, S380, and S386 were mutated to alanine and phosphomimic aspartic acid (S359D) residue. The mutated MYC-PDE8A constructs (*A*) and FLAG-PDE8A (*B*) were coexpressed with HA-14-3-3ζ in HEK293T, followed by immunoprecipitation with anti-HA antibody. *C*, WT and R56A/60A 14-3-3ζ was overexpressed with MYC-PDE8A. 14-3-3ζ was immunoprecipitated with anti-HA antibody and pull down was checked with anti-MYC/anti-FLAG antibody. GAPDH was used as the loading control. *D*, CD spectroscopy revealed relative changes in the secondary structure of the 14-3-3ζ protein upon interaction with the KA14P peptide and vice versa. The *left figure* shows CD spectra of the 14-3-3ζ protein in free and KA14P-peptide bound states. The *right* one shows CD spectra of the KA14P peptide in the absence and presence of the protein 14-3-3ζ. Protein and peptides were in a pH 6.1 buffer containing 10 mM Na_2HPO_4 and 100 mM NaCl. *E*, the HMQC spectra of the KA14P peptide were obtained both in the presence (*blue*) and absence (*red*) of the 14-3-3ζ protein. The involvement of residue pS359 and G358 in the interaction with the 14-3-3ζ protein has been indicated by the observed downfield chemical shift change. *Fi*, the ^{31}P NMR spectra have been obtained to demonstrate the interaction between KA14P peptide and the 14-3-3ζ protein. The results presented in the figure illustrate the alterations detected in the ^{31}P NMR spectra of KA14P upon the gradual addition of protein in a concentration-dependent manner. *Fii*, *graphical representation* of the alteration in the ^{31}P NMR chemical shift as a function of protein concentration. The data exhibits a sigmoidal progression. *G*, molecular recognition of phosphorylated S359 substrate protein *via* conserved polar contacts with guanidine atoms of R56, R127, and Y128 residues of 14-3-3ξ. Additional polar contacts involving (a) R5 (R355) of peptide with carboxyl side chain atoms of D223, (b) K13, A14 residues from the peptide residues maintain polar contacts with R41, N42, D213 main chain amide group atoms, and (c) K7 peptide residue also engages in polar interaction with E180 residues, bolstering the stability the substrate interaction (peptide labeling not shown for clarity). HA, hemagglutinin; NT, nontransfected cell control; PDE8A, phosphodiesterase 8A.

replacement with phospho-mimetic aspartic acid (S359D) retains the ability to interact, emphasizing the importance of phosphorylation for this interaction (Fig. 4, *A* and *B*). 14-3-3 binds to the phosphorylated protein, usually with its conserved Arg 56/60 (R56/R60) residues (25). Thus, both Arg residues were simultaneously substituted with Ala (R56A/R60A), and the interaction was tested by co-IP in HEK293T cells to see if the R56/R60 residues of 14-3-3 were involved in interacting with PDE8A. The mutant 14-3-3 does not interact with PDE8A, suggesting that the positively charged groove of 14-3-3 is essential for binding (Fig. 4*C*, lane 4).

The importance of PDE8A phosphorylation at Ser359 for interaction with 14-3-3 was then investigated biophysically using purified recombinant 14-3-3ζ. Nonphosphorylated (hereafter denoted as KA14, K^{353}DRRKG**S**LDVKAVA^{366}) and phosphorylated (hereafter denoted as KA14P, K^{353}DRRKGp**S**LDVKAVA^{366}) PDE8A peptides were synthesized around the Ser359 residue for biophysical analysis. CD spectroscopic study of 14-3-3ζ protein shows two sharp minima at 222 nm and 208 nm (Fig. 4*D*), a signature of a helical secondary structure consistent with the crystal structure (PDB: 4IHL) (26). The intensities of the two negative minima were increased further upon the addition of the KA14P peptide at a molar ratio of 1:2, suggesting the possible interaction between the KA14P peptide and the 14-3-3ζ protein, but without significant transformation of the protein's secondary structure. On the other hand, as shown in the CD spectra, KA14P alone exhibits a random coil structure with a negative maximum at around 195 nm. Interestingly, upon addition of 1 μM 14-3-3ζ protein, the spectral signature substantially shifted to a smaller negative shoulder of about 220 nm, and the negative minima have moved to a wavelength of about 205 nm (Fig. 4*D*). Here, the raw spectral data of the 14-3-3ζ protein was subtracted. This result demonstrates that the secondary conformation of KA14P acquires a portion of its helicity and produces a subpopulation of other minor conformations in the presence of 14-3-3ζ protein. In contrast, we did not observe any significant change in CD spectroscopy in the case of nonphosphorylated peptide, KA14 (Fig. S3).

Next, we performed two-dimensional ^{1}H-^{15}N heteronuclear multiple quantum coherence (HMQC) NMR analysis on the KA14P peptide, harnessing the inherent prevalence of the ^{15}N proton through nonuniform sampling acquisition (27) in the absence as well as in the presence of 14-3-3ζ. As depicted in Figure 4*E*, a visible chemical shift perturbation was observed for pSer359 (phosphorylated Ser359) and it's adjacent Gly358 residue, implying their engagement in the interaction. On the other hand, the interaction of ^{15}N labeled dimeric 14-3-3ζ protein with KA14P was difficult because of the broadening of NMR peaks (higher T_2 relaxation effect) of 14-3-3ζ protein as well as the precipitation of the 14-3-3ζ protein even at very low concentration under *in vitro* conditions (upon addition of KA14P) (Fig. S4). To further evaluate the specific interaction between pSer395 and 14-3-3ζ, one-dimensional ^{31}P NMR (28) experiment was executed (Fig. 4*F*). Addition of increasing concentration of 14-3-3ζ protein resulted in a marked change of the ^{31}P chemical shift (Fig. 4*F*i) of pSer395. This downfield shift was accentuated with increasing protein concentration, highlighting the probability of electrostatic interaction between the phosphate groups and the Lys/Arg side chains within the protein. The alteration in the ^{31}P NMR chemical shift is graphically represented in correspondence with the augmented protein concentration, culminating in a sigmoidal progression (Fig. 4*F*ii). The apparent K_D' for the interaction of KA14P and 14-3-3ζ protein is found to be 11.28 ± 0.18 μM.

Next, docking of KA14P peptide to 14-3-3ζ protein and a 200 ns molecular dynamics (MD) simulation analysis of the complex clearly suggested the peptide was able to orient into a substrate pocket with a predicted ΔG of −90.12 kcal/mol. The phosphorylated S359 mediates the key interactions of phosphate group with R56, R127, Y128 residues (Fig. 4*G*). In addition to these conserved contacts, multitude of polar contacts such as D11 (D361) carboxyl group (on peptide) interacted with amine group of K49 and, R5 (R355) guanidine atoms engage in a salt bridge interaction with carboxy (COOH) group of D223. While the K13 (363), A14 (364) main chain atom of the peptide interactions with R41, N42, and D13 side chain atoms, respectively. Most of these polar contacts were stably maintain throughout the 200 nanosecond MD simulation time frame (Figs. S5 and S6) and could further bolster the interaction with 14-3-3 ζ protein and in agreement with our experimental data and that were described previously (29). Our data, taken together, suggests that phosphorylated Ser359 of PDE8A docks to the well-conserved electropositive substrate pocket and varying such electropositive R56 or even R60 residues of 14-3-3ζ abrogates this essential protein–protein interaction.

14-3-3ζ regulates the cross-talk between cAMP/PKA and MAPK signaling through PDE8A

To find out more about the role of 14-3-3ζ in PDE8A regulation, we assessed the PDE activity of PDE8A in the presence of overexpressed 14-3-3ζ in HEK293T cells. Empty vector, PDE8A alone, or PDE8A in combination with 14-3-3ζ were transfected and treated with IBMX, a broad-spectrum PDE inhibitor. PDE8A will be active in IBMX-treated cells since it is insensitive to IBMX, whereas the function of other PDE isoforms will be inhibited. Thus, PDE8A's PDE activity will be the sole source of AMP production in IBMX-treated cells. Surprisingly, 14-3-3ζ reduced PDE8A activity (measured as total AMP generated in cells) compared to the control, implying that 14-3-3ζ inactivates PDE8A (Fig. 5*A*). The lower PDE activity of PDE8A in the presence of 14-3-3ζ is intriguing and in contrast to PDE3B, where 14-3-3β was shown to boost enzymatic activity (9).

Reduced PDE activity in cells implies an alteration in PKA signaling; therefore, changes in the phosphorylation of CREB, a PKA substrate, was investigated. In fact, an increase in CREB phosphorylation and activity was noted when PDEs were inhibited (30). So, in IBMX-treated cells where 14-3-3ζ and PDE8A are expressed alone or together, we looked for any change in the level of CREB phosphorylation to ascertain the influence of 14-3-3ζ on PDE8A activity in cells. In agreement

with the activity assay, CREB phosphorylation was significantly higher in PDE8A and 14-3-3ζ cotransfected cells in comparison to PDE8A alone, indicating that PDE8A is less active when 14-3-3ζ is present (Fig. 5*B*, lanes 3 and 4, top panel). As a control overexpression of DN-PDE8A having no enzymatic activity shows higher CREB phosphorylation than PDE8A alone (Fig. 5*B*, lane 5). Furthermore, we observed delayed CREB dephosphorylation (75 min) compared to control (30 min) and PDE8A alone (15 min) when 14-3-3ζ was overexpressed with PDE8A in forskolin treated cells (Fig. 5*C*, top panel). Delayed CREB dephosphorylation was also observed in cells overexpressing 14-3-3ζ alone, indicating a possible impact on endogenous PDE8A's basal activity in cells (Fig. S7). This data validates our previous observation that 14-3-3ζ aids in the sustenance of the PKA pathway by decreasing PDE8A activity.

It is interesting to note that in 14-3-3ζ and PDE8A cotransfected cells, inhibitory phosphorylation at Ser259 of CRAF was enhanced (Fig. 5*B*, third panel from top). This observation suggests that when 14-3-3ζ is present, PDE8A promotes signaling *via* the cAMP–PKA axis while suppressing signaling through the MAPK pathway. To support this claim, we checked if the coexpression of 14-3-3ζ and PDE8A could prevent PDE8A from activating the MAPK pathway following treatment with the MAPK pathway activator PMA. As expected, PDE8A expression alone boosted phosphorylation of extracellular signal-regulated kinase (ERK) (18), which reduced significantly upon 14-3-3ζ coexpression (Fig. 5*D*, lanes 4 and 5, top panel). In contrast, silencing of 14-3-3ζ resulted in increased ERK phosphorylation synergistically in cells expressing PDE8A (Fig. 5*E*, top panel). Notably, the expression of 14-3-3ζ alone lowered ERK phosphorylation to a certain extent (Fig. 5*D* lane 3, top panel), inversely, silencing of 14-3-3ζ facilitated ERK phosphorylation (Fig. 5*E* lane 4, top panel) emphasizing the effect of 14-3-3ζ on basal activity of PDE8A. However, after PMA treatment, DN-PDE8A could not significantly impact the phosphorylation of ERK, consistent with the earlier study where it was found to affect only the resting phospho-ERK levels (18). In light of this, our findings demonstrate that 14-3-3ζ is a key regulator of PDE8A's PDE activity, which may be essential to maintain optimal signal transmission across the cAMP/PKA and the MAPK pathways in response to distinct signaling cues.

14-3-3ζ associates with PDE8A–PRKAR1A complex in cells

Next, we looked for any direct links between PDE8A–14-3-3ζ interaction and PKA signaling, as PDE8A overexpression in the presence of 14-3-3ζ increased signaling through the PKA pathway. An *in vitro* study demonstrated the involvement of PDE8A in the hydrolysis of cAMP bound to the regulatory subunit of PKA that separates from the catalytic subunit upon cAMP binding (31). In order to corroborate these findings *in vivo*, we confirmed the interaction of PDE8A with R1α (PRKAR1A, type 1A regulatory subunit of PKA) in HEK293T cells (Fig. 6*A*). This interaction (of R1α with PDE8A) was further examined in the presence of 14-3-3ζ in order to determine the involvement of 14-3-3ζ in the formation of the PDE8A–R1α complex. Surprisingly, binding of R1α with 14-3-3ζ was not observed (Fig. 6*B*, lane 3, second panel) instead, enhanced interaction of R1α and PDE8A was found when 14-3-3ζ is overexpressed (Fig. 6*B*, lanes 4 and 5, top panel). This result suggests that 14-3-3ζ remains in the PDE8A–R1α complex. As a result of this interaction, 14-3-3ζ may aid in keeping PDE8A inactive to enhance signaling through the cAMP/PKA pathway. Collectively, our study demonstrates a novel role of 14-3-3ζ in the maintenance of the PKA pathway by modifying the PDE8A–R1α interaction and PDE8A activity.

Discussion

The cAMP signaling pathway regulates cellular proliferation, apoptosis, and differentiation by activating cAMP-dependent PKA. Hence, cAMP signaling is tightly controlled to obtain signal specificity. Though compartmentalization of cAMP has been reported for localized function, how different players affect these membraneless subcellular microdomains is still obscure. Here, we propose 14-3-3ζ as an important intrinsic factor that is a part of cAMP regulation to achieve optimal signaling through the cAMP–PKA axis.

PDEs are an important regulator of the PKA pathway, which can hydrolyze cAMP, thereby acting in the termination phase of cAMP signaling. It is particularly noteworthy that PDE8A isoform has 40- to 100-fold greater affinities for cAMP than PDE4, another cAMP-degrading enzyme (32, 33). Hence, PDE8A is more likely to be involved in resetting cAMP to basal level following activation of adenylate cyclase by G protein–coupled receptor. Indeed, as mentioned earlier, a biophysical study showed that PDE8A regulates cAMP hydrolysis by directly binding to the regulatory subunit of PKA (R1α) that dissociates from its catalytic subunit during activation of PKA signaling (31). Interestingly, a marked increase in the enzymatic activity of PDE8A was observed when it is in complex with R1α. According to the proposed model, PDE8A binds to the cAMP bound R1α as a dimer and forms a channel through the PDE8–R1α complex, acting as a new enzymatic centre to hydrolyse cAMP through substrate channelling (34). After PDE8A dissociation, the catalytic subunit rejoins R1α, and cAMP signaling is reset for another activation cycle (Fig. 7).

Here, we show 14-3-3ζ is an integral part of signaling *via* the cAMP–PKA axis by limiting PDE8A's ability to degrade cAMP. Scaffold protein 14-3-3 regulates various signaling networks (35, 36). Initially considered merely an abundant protein in the brain, 14-3-3 is now known to play a key role in regulating the location, dimerization, activation, inactivation, and degradation of its interacting partner (37, 38). It majorly binds to phosphorylated motifs on its target though it may bind to unphosphorylated targets in some cases (39). Our findings reveal that the yeast and mammalian 14-3-3 isoforms form a complex with PDE8A, a regulator of the PKA pathway, implying that it is involved in PKA signaling (Fig. 1, *A–D*). The enhancement in the interaction of PDE8A with 14-3-3ζ observed when the PKA pathway is activated supports our claim (Fig. 3*A*). Our co-IP experiment and

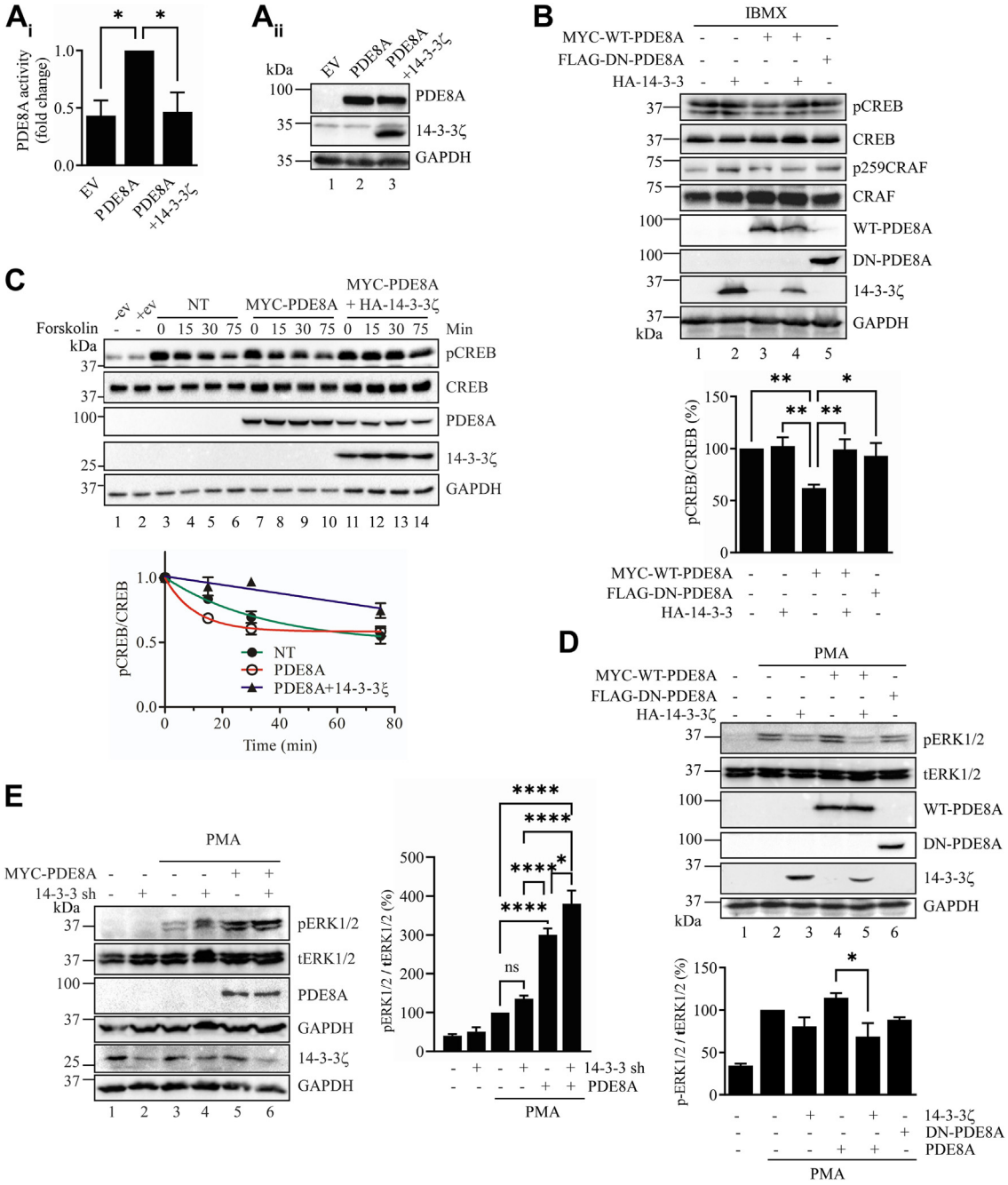

Figure 5. 14-3-3ζ decreases phosphodiesterase activity of PDE8A. *A*, PDE8A alone or with 14-3-3 was transfected into HEK293T cells. After 48 h, cells were treated with IBMX (100 μM) for 10 min. Phosphodiesterase activity was evaluated using the AMP-GLO assay kit (Promega). The *bar graph* depicts the fold change in PDE8A activity (n = 3) (*Ai*). The expression of individual proteins in cell lysates used for the AMP-GLO assay is shown by Western blot (*Aii*). *B–D*, in HEK293T cells, HA-14-3-3ζ, MYC-PDE8A, and DN-PDE8A were transfected alone or 14-3-3ζ and PDE8A together and treated with IBMX (100 μM) for 10 min to block other PDEs except PDE8A (*B*) or PMA (1 μM) for 15 min to stimulate ERK signaling (*D*). HEK293T cells overexpressing HA-14-3-3ζ and MYC-PDE8A alone or in combination were treated with 100 μM forskolin (15 min) to activate the PKA pathway before being harvested at 0, 15, 30, and 75 min time point after media change (*C*). *E*, MYC-PDE8A was transfected in WT and 14-3-3ζ shRNA stable HEK293T cells and treated with PMA (1 μM) as indicated. The band intensity of pCREB (*B* and *C*) and pERK1/2 (*D* and *E*) was quantified, normalized to tCREB and tERK1/2, respectively, and represented in the adjacent graph. n = 3 (*A–D*), n = 4 (*E*). *Histobars* represent mean ± SEM. One-way ANOVA was used to determine significance, $*p < 0.05$. $**p < 0.01$, $***p < 0.001$, and $****p < 0.0001$. WT-PDE8A, DN-PDE8A, and 14-3-3ζ expression was validated in the cell lysates with anti-MYC, anti-FLAG, and anti-HA antibodies, respectively. 14-3-3ζ level in shRNA stable cell was confirmed using endogenous 14-3-3ζ antibody. GAPDH served as the loading control for each experiment. ERK, extracellular signal-regulated kinase; EV, empty vector; HA, hemagglutinin; IBMX, 3-isobutyl-1-methylxanthine; NT, nontransfected cell control; PDE8A, phosphodiesterase 8A.

biophysical studies have established that 14-3-3ζ, irrespective of its dimerization status, binds to PDE8A if PKA phosphorylates its Ser359 residue (Figs. 1*E* and 4, *B*, *D*, *E*, and *G*). As an obligatory dimer (Fig. S1), 14-3-3ζ can interact with two phosphorylated motifs on a single target simultaneously or link phosphorylated motifs on two different binding partners (40). On the other hand, dimerization of PDE8A from a cellular standpoint is not yet conclusive, but

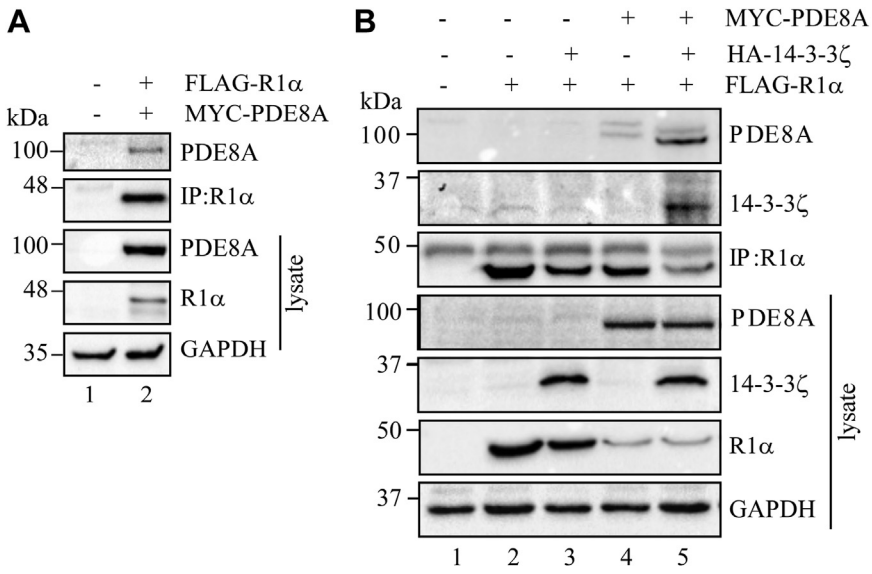

Figure 6. R1α increases its association with PDE8A in the presence of 14-3-3ζ. *A*, FLAG-R1α was transfected with MYC-PDE8A in HEK239T cells. *B*, FLAG-R1α was expressed alone or in combination with HA-14-3-3ζ, MYC-PDE8A, or both in HEK293T cells. R1α was pulled with anti-FLAG antibody. Immunoprecipitate and the total lysate were checked with anti-MYC, anti-HA, and anti-flag antibodies. GAPDH was the loading control. PDE8A, phosphodiesterase 8A.

hydrodynamics evidence and the model put forth by Tulsian *et al.* point to such possibility (31, 34, 41). The identification of a single phosphorylated residue of PDE8A in our study that interacts with 14-3-3ζ thus suggests that one 14-3-3ζ dimer may hold two PDE8A monomers together, altering their enzymatic activity. Moreover, a single interaction site should allow 14-3-3ζ to easily dissociate from PDE8A for signal termination by the action of phosphatases. Our study further reveals that PKA activity is enhanced when 14-3-3ζ is coexpressed with PDE8A in HEK293T cells. This increased PKA activity can be attributed to the observed reduction in PDE activity of PDE8A in the presence of 14-3-3ζ (Fig. 5*A*). Increased PKA activity in cells overexpressing 14-3-3ζ with PDE8A, activates its downstream target CREB (Fig. 5*B*), a transcription factor important in many cellular processes such as proliferation and survival. Thus, the present study reveals a novel role for 14-3-3ζ in the activation phase of cAMP-PKA signaling. In other words, the reduced activity of PDE8A when it is expressed with 14-3-3ζ constitutes a counter feedback mechanism to delay the degradation of cAMP by PDE8A or PDE8A–R1α complex to maximize signal output following a hormone stimulus. This is reasonably logical because PKA initiates its deactivation by increasing the enzymatic activity of PDE8A by phosphorylating it. A recent study found that R1α undergoes liquid–liquid phase separation to generate a distinct cAMP compartment capable of retaining high cAMP and PKA activity (42). Interestingly, 14-3-3 also has a high potential to regulate the function of its target protein undergoing liquid–liquid phase separation (42). The delayed termination of PKA signaling by PDE8A as well as the increased PDE8A–R1α interaction in the presence of 14-3-3ζ, suggest that 14-3-3ζ sequesters PDE8A in the cellular microenvironment (Figs. 5*C* and 6*B*). Thus, 14-3-3 may be a part of this landscape which helps to retain cAMP and PKA activity by suppressing PDE8A activity in specialized phase-separated compartments (43). Strikingly, it was interesting to note that the PDE8A K14P peptide segment itself was sufficient for recognition of 14-3-3ζ and influence the downstream signaling of PDE8A–14-3-3ζ axis and future research may offer more insight into this unexplored prospect.

The antagonistic role of cAMP-PKA signaling on the MAPK pathway is well documented (44). 14-3-3ζ has a dual influence on CRAF kinase involved in the MAPK pathway, activating at phosphorylated Ser621 and inhibiting at phospho-Ser259 residue (45). High PKA activity turns down the MAPK pathway by adding a phosphate group to inhibitory Ser259 residues of CRAF, allowing the binding of 14-3-3ζ at this site. 14-3-3ζ binding at phospho-Ser259 locks CRAF in an inactive state and blocks its interaction with rat sarcoma (RAS), an obligatory requirement for the activation of MAPK pathway (44). For many years, the above mentioned CRAF inactivation by PKA was the only known mechanism by which the cAMP/PKA axis negatively impacts MAPK. Later, it was discovered that PDE8A restricts PKA from inactivating CRAF by binding to it and hydrolyzing the local cAMP pool, thereby enhancing MAPK signaling. Nonetheless, it is unclear how PDE8A's enzymatic activity is controlled because it stays in a complex with CRAF, which may end in improper activation of the MAPK pathway. This is reflected in the fact that deleting PDE8A alone reduces MAPK signaling in *Drosophila* and mice (18). 14-3-3ζ promotes phosphorylation at Ser259 by reducing the enzymatic activity of PDE8A surrounding CRAF, which decreases signal transmission to ERK1/2 down the MAPK pathway (Figs. 5*D* and 7), presumably by preventing RAS association (44). The association of 14-3-3ζ with PDE8A altering its activity demonstrated in our study thus represents a counter mechanism by which the capacity of the cAMP/PKA pathway to inhibit MAPK pathway is increased in response to various signaling/hormonal cues (Fig. 7).

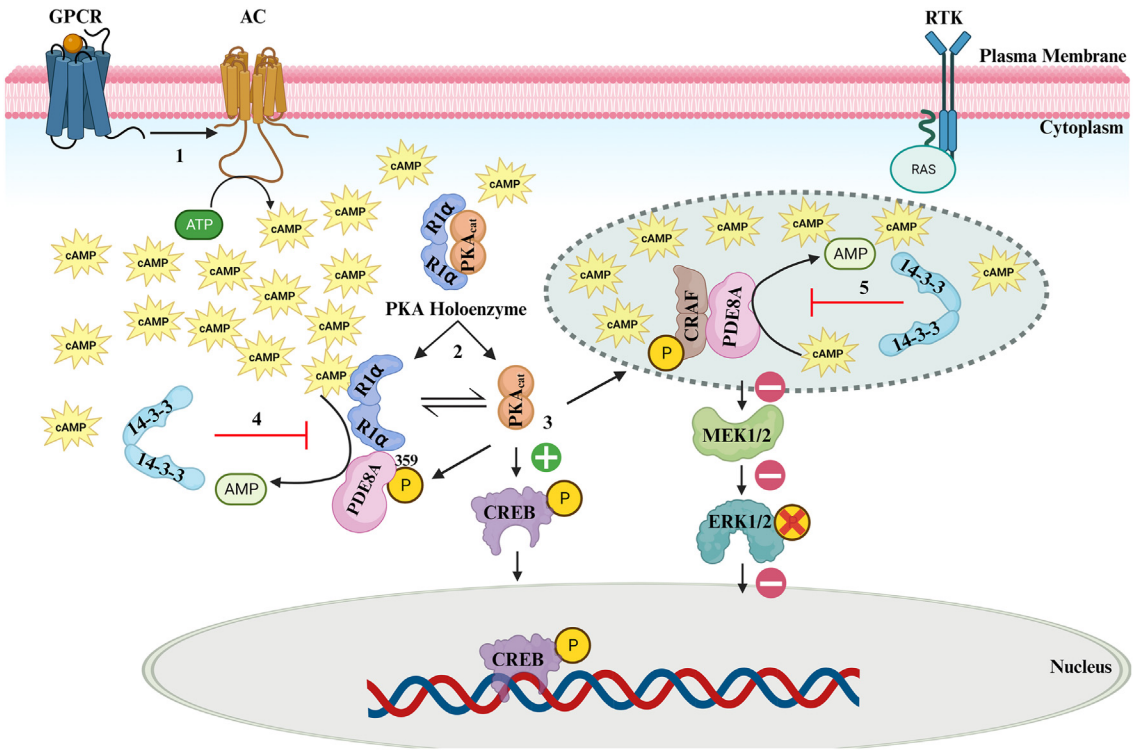

Figure 7. Proposed model for the role of 14-3-3ζ in regulation of PDE8A activity and downstream signaling. 1, binding of ligand to the membrane bound G protein–coupled receptor (GPCR) activates adenylate cyclase (AC). Activated AC converts ATP to cAMP. 2, cAMP thereby binds to the regulatory subunit (R1α) of PKA and facilitates dissociation of the catalytic subunit (PKA_{cat}). 3, PKA_{cat} in turn phosphorylates CREB, PDE8A, and CRAF at Ser133, Ser359, and Ser259 residues, respectively. Phosphorylated CREB moves to the nucleus and promotes transcription of target genes. On the other hand, activated PDE8A binds to R1α and begins hydrolyzing cAMP by substrate channeling, thereby turning down the PKA signal. In addition, phosphorylation of CRAF facilitates 14-3-3ζ binding and inactivates MAPK pathway. 4, binding of 14-3-3ζ to the phosphorylated Ser359 residue of PDE8A, inhibits its phosphodiesterase activity and sustains the cAMP/PKA/CREB cascade. 5, in subcellular microdomains, 14-3-3ζ enhances the cAMP pool by inhibiting PDE8A activity associated with CRAF and promote inhibitory Ser259 phosphorylation of CRAF by PKA_{cat}, thus downregulating of MEK/ERK pathway. The model was created using BioRender. ERK, extracellular signal-regulated kinase; MAPK, mitogen-activated protein kinase; PDE8A, phosphodiesterase 8A.

The RAS-RAF-MEK-ERK cascade is altered in many cancers due to mutation in RAS and RAF isoforms (46). Despite the tremendous potential, direct RAF inhibition has limitations since RAF inhibitors transactivate RAF dimers and stimulate the MAPK pathway, resulting in drug resistance and tumor relapse (47–49). On the contrary, increasing cAMP/PKA signaling by directly inhibiting PDE has been beneficial in the treatment of inflammatory disorders (4, 50). Compounds that stabilize 14-3-3 protein–protein interactions (PPIs) have lately garnered substantial research due to their role in changing the function of various disease-causing proteins (51). For instance, PPI stabilizers of 14-3-3 with estrogen receptor alpha that negatively regulates the function of estrogen receptor alpha are being considered as a potential breast cancer therapy (52). In this regard, our findings, which redefine 14-3-3's role as a molecular switch enhancing, signaling through the PKA pathway and restricting the MAPK pathway by serving as an endogenous PDE8A inhibitor, imply that the PDE8A-14-3-3 PPI stabilizer could be relevant for future drug discovery.

Experimental procedures

Reagent and chemicals

Forskolin (#F3917), H-89 dihydrochloride hydrate (#B1427), phorbol 12-myristate 13-acetate (PMA, #P8139), GF 109203X hydrochloride (#B6292), and human insulin (#91077C) were purchased from Sigma Aldrich Co. Pilaralisib (#XL147) (Selleck Chemicals LLC) was a kind gift from Dr Nirmalya Sen (Bose Institute). Bicinchoninic acid (BCA) protein estimation kit was purchased from Thermo Fisher Scientific. HPLC-purified (>95%) KA14 and KA14P peptides having the following sequence were commercially synthesized from GenScript Biotech Corporation.

KA14-K^{353}DRRKGSLDVKAVA^{366}

KA14P-K^{353}DRRKG**S**LDVKAVA^{366}, the highlighted and underlined Ser359 residue is phosphorylated.

Plasmids, cloning, and protein purification

HA-tagged 14-3-3 isoforms, β, η, ε, σ, DN-14-3-3R56/60A, and pDONR223-PRKAR1A are obtained from Addgene, (#13270, #116887, #116886, #11946, #116889, #23741). pCDNA3.1 FLAG-PDE8A construct was obtained from GenScript (#OHu13098D). MYC-PDE8A and FLAG-PRKAR1A were subcloned in pCDNA3.1 vector with Addgene constructs as templates. DN-PDE8A was cloned as previously reported (18). Yeast homologue of 14-3-3, *BMH1*, and *BMH2* were cloned in pRS416-GPD vector with HA-tag by PCR using yeast genomic DNA as template with the following primers:

BMH1-F- 5′ CGCGGATCCATGTACCCATACGATGTT CCAGATTACGCTATGTCAAC.

CAGTCGTGAAG, BMH1-R-5′-CCGGAATTCTTACTTT GGTGCTTC; BMH2-F5′-CCAT.

GTACCCATACGATGTTCCAGATTACGCTATGTCCC AAACTCGTGAAG, BMH2-R-5′-CCGGAATTCTTATTT GGTTGGTTC.

WT and monomeric (^{12}LAE^{14} → ^{12}QQR^{14}) human 14-3-3ζ bacterial constructs were a gift from Dr Nikolai Sluchanko, Federal Research Centre of the Russian Academy of Sciences. HA-tagged and monomeric 14-3-3ζ (14-3-3ζm) in pCDNA3.1 vector were generated using bacterial constructs as a template.

Human 14-3-3ζ was purified as described (53). Briefly, 14-3-3ζ-pQE30 transformed in *Escherichia coli* M15 cells was induced with 0.5 mM IPTG for 3 h at 37 °C. Cells resuspended in 100 mM sodium phosphhate buffer (pH 7.4) with 300 mM NaCl, 1 mM PMSF and protease inhibitor cocktail were lysed with French press at 20,000 psi. The clarified lysate was applied to nickel-nitrilotriacetic acid column and the protein was eluted with 10 mM imidazole in lysis buffer. The protein was subjected to dialysis to remove imidazole, concentrated and stored in −80 °C in storage buffer containing 10 mM phosphate buffer pH 6.1 and 50 mM NaCl. For ^{15}N labeling, *E. coli* M15 cells expressing His-14-3-3ζ was grown in M9 minimal media containing 5 × M9 (Na_2HPO_4, KH_2PO_4, NaCl), 0.25 g/ml $^{15}NH_4Cl$, 0.1% glucose, 2 mM $MgSO_4$, 100 mM $CaCl_2$, 200 µl vitamins and antibiotics. Ninety to hundred microliters of primary culture was added to 1 l of M9 media and incubated overnight with shaking (120–150 rpm). Protein was induced with 0.5 mM IPTG at A_{600} 0.6 to 0.8 for 3 h at 37 °C. ^{15}N-labeled 14-3-3ζ was purified similarly as the nonlabeled protein.

Yeast cell culture

Yeast strain BY4741 (MATa his3Δ0 leu2Δ0 met15Δ0 ura3Δ0) was used in this study. *bmh1Δ* and *bmh2Δ* yeast strains were obtained from the yeast knockout library. Yeast transformation was carried out as described previously (54).

Mammalian cell culture and transfection

HEK293T, HCT116, and MCF7 were purchased from National Centre for Cell Science. HEK293T and HCT116 cells were maintained in Dulbecco's modified Eagle medium (Gibco, Thermo Fisher Scientific). MCF-7 cell line was cultured in RPMI media (Gibco, Thermo Fisher Scientific). Cells were supplemented with 10% fetal bovine serum (Gibco, Thermo Fisher Scientific) and kept in a humidified incubator with 5% CO_2. Plasmid DNAs were transfected with PEI (Polysciences, Inc) at 70% confluence in opti-Minimal Essential Medium (Gibco, Thermo Fisher Scientific) without serum.

Western blotting and IP

HEK293T cells were lysed with radioimmunoprecipitation assay buffer containing 50 mM Tris–HCl (pH 7.5), 150 mM NaCl, 1 mM EDTA, 0.1% SDS, and 1 mM PMSF with protease inhibitor cocktail. Yeast cells were lysed in the same buffer with glass beads by giving 30 s pulse in bead bitter at 4 °C. Cell lysates were centrifuged at 13,000*g* for 30 min at 4 °C, followed by protein estimation of clarified lysate by BCA. The proteins were separated by 8 to 10% SDS-PAGE and transferred onto a nitrocellulose membrane (Pall Corporation). The membrane was blocked with 5% nonfat milk for 1 h followed by overnight incubation by the following primary antibodies, α-FLAG (Sigma, F7425), α-HA (Sigma, H3663), α-MYC (Merck, #05-724), α-14-3-3 pan (CST, #8312), α-14-3-3ζ (CST, #9639), α-GAPDH (BioBharati LifeScience, BB-AB0060), α-p-ERK1/2 (CST, #4370), total ERK1/2 (CST, #4696), α-pCREB (CST, #9198), total CREB (CST, #9197), α-p-Ser259 CRAF (CST, #9421), α-CRAF (BD Biosciences, 610152), α-GFP (Roche, 11814460001), α-HIS (Sigma, H1029), and α-PGK1 (Invitrogen, 459250). The next day the blots were washed thrice with 1x Tris buffer containing 0.1% Tween 20 for 10 min, followed by incubation with horseradish peroxidase-labeled secondary goat α-mouse IgG and goat α-rabbit antibodies (Jackson Laboratory) for 1 to 2 h. The proteins were visualized using enhanced chemiluminescence detection buffer, and the image was captured in the Chemidoc MP system (Bio-Rad).

For IP, HEK293T and yeast cells were lysed in a buffer containing 50 mM Tris, pH 7.5, 150 mM NaCl, 0.1% SDS, 0.5% Triton X-100, 5% glycerol, 1 mM PMSF, and protease inhibitor cocktail. Lysate was clarified by centrifugation at 13,000*g* for 30 min at 4 °C, followed by protein estimated by the BCA method. The cell lysates were incubated with antibodies in IP dilution buffer (50 mM Tris, pH 7.5, 150 mM NaCl, 0.1% Triton X-100, PMSF) overnight at 4 °C with gentle rotation. The next day, protein A-Sepharose (GE Healthcare) bead pre-equilibrated with IP dilution buffer was added and incubated further with rotation for 2 h at 4 °C for IP. The beads were then washed three times with IP dilution buffer. Bound proteins were eluted from beads with SDS sample buffer, vortexed, boiled for 5 min, and analyzed by Western blotting.

Generation of CRAF knockout and 14-3-3ζ shRNA stable HEK293T cell

CRAF knockout HEK293T cell was generated by CRISPR/Cas9 system, using guide RNA targeting exon 4 of CRAF (sense oligo: 5′-CACCGACTGATGCTGCGTCTTTGAT-3′ and antisense oligo: 5′-AAACATCAAAGACGCAGC ATCAGTC-3′) and cloned into pSpCas9(BB)-2A-Puro (PX459) V2.0, obtained from Addgene (#62988). Cells were then transfected with the cloned plasmid, and media was changed with complete Dulbecco's modified Eagle medium after 6 h of transfection. Puromycin (0.75 µg/ml) was added after 48 h of transfection and the cells were cultured for 12 days, before colony picking and monoclonal expansion. Targeted region and predicted off-target exons were checked from monoclone 1 by sequencing, which is used for the experiments.

Sequence for 14-3-3ζ shRNA was obtained from previously reported siRNA sequence (55). 14-3-3ζ shRNA was cloned into pLKO.1-TRC (#10878, Addgene) lentiviral backbone according to the protocol (Addgene) for producing lentiviral

particles. The shRNA construct was transfected with packaging and envelop plasmids, psPAX2 (#12260) and pMD2.G (#12259), respectively in HEK293T for virus production. Virus particles were added to exponentially growing cells and treated with puromycin (0.75 μg/ml) for selection of stable cell line.

Circular dichroism

The Jasco J-815 spectrophotometer was utilized to investigate the secondary structures of the peptide KA14P and the protein 14-3-3ζ. A buffer consisting of 10 mM Na_2HPO_4 and 100 mM NaCl with a pH of 6.1 was utilized throughout the study. All spectra were obtained using a quartz cuvette with a path length of 0.2 cm at a temperature of 298 K for 25 μM KA14P without or with 1 μM of 14-3-3ζ protein. The spectra were recorded either in the absence or presence of 14-3-3ζ protein. Spectra were recorded between 196 and 260 nm of wavelength using a scanning speed of 100 nm/min and a data interval of 0.1 nm. Every CD spectrum is the result of adding together three successive scans. The CD spectra were corrected for background noise by subtracting the CD spectra of the same concentration of protein (without KA14P) from those obtained. Ellipticity in molar units was calculated by subtracting the blank buffer data (in millidegrees) from the raw spectral data using the following equation.

$$Molar\ ellipticity(\theta) = \frac{m_0 M}{10} L \times C$$

where m_0 represents millidegrees, M represents molecular weight (g mol^{-1}), L represents the path length of the quartz cuvette utilized (cm), and C represents concentration (molarity).

Nuclear magnetic resonance

Two-dimensional ^{1}H-^{15}N HMQC NMR and ^{31}P NMR techniques were implemented using a Bruker AVANCE III 700 MHz and 500 MHz NMR spectrometer, equipped with room temperature and 5 mm SMART probe, respectively. The accompanying software, Topspin v3.1 (Bruker Biospin GmbH; https://www.bruker.com/topspin), facilitated both data acquisition and subsequent processing. In all our NMR studies, 4,4-dimethyl-4-silapentane-1 sulfonic acid was used as the internal standard, allowing for precise chemical shift referencing.

For HMQC NMR, the procedure exploited the natural abundance of the ^{15}N proton through nonuniform sampling acquisition, examining the KA14P peptide both in the absence and presence of 14-3-3ζ protein at 298K.

The ^{31}P NMR spectra were recorded at 288 K with varying concentrations of the 14-3-3ζ protein, dissolved in deionized water, and pH was adjusted to 6.1. The peptide concentration was set at 500 μM. Spectra were acquired with 512 scans, 16 dummy scans, and incorporated a 10 s recycle delay between each recording. Pre-transformation of the spectra *via* Fourier methods involved applying an exponential line-broadening function of 20 Hz to each dataset, which improved the signal-to-noise ratio. To elucidate the K_d for our peptide–protein interaction study, we adopted a comprehensive methodological approach. The protein concentrations were entered in the X-column, and the corresponding specific binding measurements (peak intensity) were recorded in the Y-column. With our binding data, we proceeded to apply nonlinear regression analysis using the Hill equation model. This model is explicitly chosen for its applicability to saturation binding studies and is represented by the equation:

$$Y = \frac{B_{max}.X^h}{K_d^h + X^h}$$

where Y signifies the specific binding, B_{max} is the maximum specific binding achievable, X denotes the protein concentration, K_d is the concentration at which half-maximum binding is observed, and h represents the Hill slope, indicating the degree of cooperativity in the binding interaction.

Molecular modeling studies

Protein preparation

The crystal structure of receptor 14-3-3 ζ protein in complex with a CRAF phosphopeptide (PDB 4IHL (29), A subunit) was utilized for receptor preparation. During these steps, multiple conformations of residues, missing atoms, overlapping atoms, and any bond orders were corrected. The heteroatoms were removed, and the added hydrogen atoms were energy minimized using a restrained minimization using OPLS 2005 force-field in the protein preparation wizard in the maestro suite of programs (56).

Ligand/peptide preparation

Peptide docking: The coordinates of phospho-substrate PDE8 protein 350 to 364 (hereafter denoted as *p*) were built by using the homology modeling on TFEB 14-3-3 binding motif coordinates (pdb 6A5S (57)). Thus, obtained bound phospho-substrate (KA14P) peptide was energy minimized using the protein preparation wizard in the Schrödinger suite of programs. Next, the receptor–peptide complex was energy minimized by prime MMGBSA with side chains refinement. Next, 200 ns MD run was carried to out to assess the stability of peptide complex using Desmond tools with Schrödinger suite of programs (56).

AMP-GLO assay

Cells for measuring PDE activity were treated with IBMX, washed three times with ice cold 1X PBS, and lysed in buffer containing 50 mM Tris pH 8, 150 mM NaCl, 1% Triton X-100, 10% glycerol, 1 mM PMSF, 1X protease inhibitor cocktail (Roche), and phosphatase inhibitor (Thermo Scientific). For the experiment, an equal amount of total protein measured by BCA method was added to a white microplate for assay. The amount of AMP in each sample was determined by AMP-GLO assay kit (Promega) according to manufacturer's protocol. The reading was taken in Luminescence reader (VARIOSKAN FLASH, Thermo Fisher Scientific). GraphPad Prism 10 (https://www.graphpad.com) was used to plot the fold change

from three different experiments. The significance was determined using one-way ANOVA with a 95% confidence interval.

Statistical analysis

Western blots were quantified using Image Lab software (BioRad Laboratories, https://www.bio-rad.com/en-in/product/image-lab-software?source_wt=imagelabsoftware_surl&ID=KRE6P5E8Z). Data from triplicate experiments were plotted as mean ± SEM in GraphPad Prism10. Significance was calculated using one-way ANOVA, where a p value less than 0.05 was considered as statistically significant.

Supporting information—This article contains supporting information.

Acknowledgments—We thank Nilanjan Gayen for his initial input on the study. We are thankful to Nikolai Sluchanko and Nirmalya Sen for gifting 14-3-3 constructs and pilaralisib, respectively.

Author contributions—A. K. M. conceptualization; A. B. and A. K. M. supervision; A. B. and A. K. M. writing-review and editing, A. K. M. funding acquisition; A. K. M. project administration; Soumita Mukherjee methodology; Soumita Mukherjee and S. R. validation; Soumita Mukherjee and Shruti Mukherjee formal analysis; Soumita Mukherjee, S. R., Shruti Mukherjee, and A. H. investigation; Soumita Mukherjee and Shruti Mukherjee writing-original draft.

Funding and additional information—This work was supported by grant from STBT-WB [1811(Sanc.)/STBT-11012(12)/23/2020-BT SEC] to A. K. M. and funding from Bose Institute Intramural fund. Soumita Mukherjee is supported by postdoctoral fellowship from Science and Engineering Research Board (SERB), Government of India. Soumita Mukherjee is grateful for the financial support from the DBT-RA Program in Biotechnology and Life Sciences. S. R. and Sh. M. thank DBT and CSIR for fellowships, respectively.

Conflict of interest—The authors declare that they have no conflicts of interest with the contents of this article.

Abbreviations—The abbreviations used are: BCA, bicinchoninic acid; ERK, extracellular signal-regulated kinase; HA, hemagglutinin; HMQC, heteronuclear multiple quantum coherence; IBMX, 3-isobutyl-1-methylxanthine; IP, immunoprecipitation; MAPK, mitogen-activated protein kinase; MD, molecular dynamics; PDE, phosphodiesterase; PPI, protein–protein interaction; RAS, rat sarcoma.

References

1. Omori, K., and Kotera, J. (2007) Overview of PDEs and their regulation. *Circ. Res.* **100**(3), 309–327
2. Bender, A. T., and Beavo, J. A. (2006) Cyclic nucleotide phosphodiesterases: molecular regulation to clinical use. *Pharmacol. Rev.* **58**, 488–520
3. Matera, M. G., Page, C., and Cazzola, M. (2014) PDE inhibitors currently in early clinical trials for the treatment of asthma. *Expert Opin. Investig. Drugs* **23**, 1267–1275
4. Matera, M. G., Rogliani, P., Calzetta, L., and Cazzola, M. (2014) Phosphodiesterase inhibitors for chronic obstructive pulmonary disease: what does the future hold? *Drugs* **74**, 1983–1992
5. Field, S. K. (2008) Roflumilast: an oral, once-daily selective PDE-4 inhibitor for the management of COPD and asthma. *Expert Opin. Investig. Drugs* **17**, 811–818
6. Dodge-Kafka, K. L., Langeberg, L., and Scott, J. D. (2006) Compartmentation of cyclic nucleotide signaling in the heart. *Circ. Res.* **98**, 993–1001
7. McConnachie, G., Langeberg, L. K., and Scott, J. D. (2006) AKAP signaling complexes: getting to the heart of the matter. *Trends Mol. Med.* **12**, 317–323
8. Onuma, H., Osawa, H., Yamada, K., Ogura, T., Tanabe, F., Granner, D. K., *et al.* (2002) Identification of the insulin-regulated interaction of phosphodiesterase 3B With 14-3-3 β protein. *Diabetes* **51**, 3362–3367
9. Palmer, D., Jimmo, S. L., Raymond, D. R., Wilson, L. S., Carter, R. L., and Maurice, D. H. (2007) Protein kinase A phosphorylation of human phosphodiesterase 3B promotes 14-3-3 protein binding and inhibits phosphatase-catalyzed inactivation. *J. Biol. Chem.* **282**, 9411–9419
10. Pozuelo Rubio, M., Campbell, D. G., Morrice, N. A., and Mackintosh, C. (2005) Phosphodiesterase 3A binds to 14-3-3 proteins in response to PMA-induced phosphorylation of Ser428. *Biochem. J.* **392**, 163–172
11. Soderling, S. H., Bayuga, S. J., and Beavo, J. A. (1998) Cloning and characterization of a cAMP-specific cyclic nucleotide phosphodiesterase. *Proc. Natl. Acad. Sci. U. S. A.* **95**, 8991–8996
12. Dong, H., Osmanova, V., Epstein, P. M., and Brocke, S. (2006) Phosphodiesterase 8 (PDE8) regulates chemotaxis of activated lymphocytes. *Biochem. Biophys. Res. Commun.* **345**, 713–719
13. Patrucco, E., Albergine, M. S., Santana, L. F., and Beavo, J. A. (2010) Phosphodiesterase 8A (PDE8A) regulates excitation-contraction coupling in ventricular myocytes. *J. Mol. Cell. Cardiol.* **49**, 330–333
14. Shimizu-Albergine, M., Tsai, L. C., Patrucco, E., and Beavo, J. A. (2012) cAMP-specific phosphodiesterases 8A and 8B, essential regulators of leydig cell steroidogenesis. *Mol. Pharmacol.* **81**, 556–566
15. Vang, A. G., Ben-Sasson, S. Z., Dong, H., Kream, B., DeNinno, M. P., Claffey, M. M., *et al.* (2010) PDE8 regulates rapid teff cell adhesion and proliferation independent of ICER. *PLoS One* **5**, e12011
16. Johnstone, T. B., Smith, K. H., Koziol-White, C. J., Li, F., Kazarian, A. G., Corpuz, M. L., *et al.* (2018) PDE8 is expressed in human airway smooth muscle and selectively regulates cAMP signaling by β2-adrenergic receptors and adenylyl cyclase 6. *Am. J. Respir. Cell Mol. Biol.* **58**, 530–541
17. Brown, K. M., Lee, L. C., Findlay, J. E., Day, J. P., and Baillie, G. S. (2012) Cyclic AMP-specific phosphodiesterase, PDE8A1, is activated by protein kinase A-mediated phosphorylation. *FEBS Lett.* **586**, 1631–1637
18. Brown, K. M., Day, J. P., Huston, E., Zimmermann, B., Hampel, K., Christian, F., *et al.* (2013) Phosphodiesterase-8A binds to and regulates Raf-1 kinase. *Proc. Natl. Acad. Sci. U. S. A.* **110**, E1533–E1542
19. Blair, C. M., Walsh, N. M., Littman, B. H., Marcoux, F. W., and Baillie, G. S. (2019) Targeting B-Raf inhibitor resistant melanoma with novel cell penetrating peptide disrupters of PDE8A - C-Raf. *BMC Cancer* **19**, 266
20. Clapp, C., Portt, L., Khoury, C., Sheibani, S., Norman, G., Ebner, P., *et al.* (2012) 14-3-3 protects against stress-induced apoptosis. *Cell Death Dis.* **3**, e348
21. Sluchanko, N. N., Artemova, N. V., Sudnitsyna, M. V., Safenkova, I. V., Antson, A. A., Levitsky, D. I., *et al.* (2012) Monomeric 14-3-3ζ Has a chaperone-like activity and is stabilized by phosphorylated HspB6. *Biochemistry* **51**, 6127–6138
22. Sluchanko, N. N., Sudnitsyna, M. V., Seit-Nebi, A. S., Antson, A. A., and Gusev, N. B. (2011) Properties of the monomeric form of human 14-3-3ζ protein and its interaction with Tau and HspB6. *Biochemistry* **50**, 9797–9808
23. Dubois, T., Rommel, C., Howell, S., Steinhussen, U., Soneji, Y., Morrice, N., *et al.* (1997) 14-3-3 Is Phosphorylated by casein kinase I on residue 233. *J. Biol. Chem.* **272**, 28882–28888
24. Obenauer, J. C., Cantley, L. C., and Yaffe, M. B. (2003) Scansite 2.0: proteome-wide prediction of cell signaling interactions using short sequence motifs. *Nucleic Acids Res.* **31**, 3635–3641
25. Thorson, J. A., Yu, L. W., Hsu, A. L., Shih, N. Y., Graves, P. R., Tanner, J. W., *et al.* (1998) 14-3-3 proteins are required for maintenance of Raf-1 phosphorylation and kinase activity. *Mol. Cell. Biol.* **18**, 5229–5238
26. Arakawa, T., Tokunaga, M., Kita, Y., Niikura, T., Baker, R. W., Reimer, J. M., *et al.* (2021) Structure analysis of proteins and peptides by difference circular dichroism spectroscopy. *Protein J.* **40**, 867–875
27. Palmer, M. R., Wenrich, B. R., Stahlfeld, P., and Rovnyak, D. (2014) Performance tuning non-uniform sampling for sensitivity enhancement of signal-limited biological NMR. *J. Biomol. NMR* **58**, 303–314

28. Ghosh, A., Datta, A., Jana, J., Kar, R. K., Chatterjee, C., Chatterjee, S., *et al.* (2014) Sequence context induced antimicrobial activity: insight into lipopolysaccharide permeabilization. *Mol. Biosyst.* **10**, 1596–1612
29. Molzan, M., Kasper, S., Roglin, L., Skwarczynska, M., Sassa, T., Inoue, T., *et al.* (2013) Stabilization of physical RAF/14-3-3 interaction by cotylenin A as treatment strategy for RAS mutant cancers. *ACS Chem. Biol.* **8**, 1869–1875
30. Xia, M., Huang, R., Guo, V., Southall, N., Cho, M. H., Inglese, J., *et al.* (2009) Identification of compounds that potentiate CREB signaling as possible enhancers of long-term memory. *Proc. Natl. Acad. Sci. U. S. A.* **106**, 2412–2417
31. Krishnamurthy, S., Moorthy, B. S., Xin Xiang, L., Xin Shan, L., Bharatham, K., Tulsian, N. K., *et al.* (2014) Active site coupling in PDE:PKA complexes promotes resetting of mammalian cAMP signaling. *Biophys. J.* **107**, 1426–1440
32. Gamanuma, M., Yuasa, K., Sasaki, T., Sakurai, N., Kotera, J., and Omori, K. (2003) Comparison of enzymatic characterization and gene organization of cyclic nucleotide phosphodiesterase 8 family in humans. *Cell. Signal.* **15**, 565–574
33. Fisher, D. A., Smith, J. F., Pillar, J. S., St Denis, S. H., and Cheng, J. B. (1998) Isolation and characterization of PDE8A, a novel human cAMP-specific phosphodiesterase. *Biochem. Biophys. Res. Commun.* **246**, 570–577
34. Tulsian, N. K., Krishnamurthy, S., and Anand, G. S. (2017) Channeling of cAMP in PDE-PKA complexes promotes signal adaptation. *Biophys. J.* **112**, 2552–2566
35. Aghazadeh, Y., and Papadopoulos, V. (2015) The role of the 14-3-3 protein family in health, disease, and drug development. *Drug Discov. Today* **21**, 278–287
36. Morrison, D. K. (2009) The 14-3-3 proteins: integrators of diverse signaling cues that impact cell fate and cancer development. *Trends Cell Biol.* **l19**, 16–23
37. Pennington, K. L., Chan, T. Y., Torres, M. P., and Andersen, J. L. (2018) The dynamic and stress-adaptive signaling hub of 14-3-3: emerging mechanisms of regulation and context-dependent protein-protein interactions. *Oncogene* **37**, 5587–5604
38. Diviani, D., Abuin, L., Cotecchia, S., and Pansier, L. (2004) Anchoring of both PKA and 14-3-3 inhibits the Rho-GEF activity of the AKAP-Lbc signaling complex. *EMBOJ* **23**, 2811–2820
39. Shen, Y. H., Godlewski, J., Bronisz, A., Zhu, J., Comb, M. J., Avruch, J., *et al.* (2003) Significance of 14-3-3 self-dimerization for phosphorylation-dependent target binding. *Mol. Biol. Cell* **14**, 4721–4733
40. Gardino, A. K., Smerdon, S. J., and Yaffe, M. B. (2006) Structural determinants of 14-3-3 binding specificities and regulation of subcellular localization of 14-3-3-ligand complexes: a comparison of the X-ray crystal structures of all human 14-3-3 isoforms. *Semin. Cancer Biol.* **16**, 173–182
41. Conti, M., and Beavo, J. (2007) Biochemistry and physiology of cyclic nucleotide phosphodiesterases: essential components in cyclic nucleotide signaling. *Annu. Rev. Biochem.* **76**, 481–511
42. Huang, X., Zheng, Z., Wu, Y., Gao, M., Su, Z., and Huang, Y. (2022) 14-3-3 proteins are potential regulators of liquid-liquid phase separation. *Cell Biochem. Biophys.* **80**, 277–293
43. Zhang, J. Z., Lu, T. W., Stolerman, L. M., Tenner, B., Yang, J. R., Zhang, J. F., *et al.* (2020) Phase separation of a PKA regulatory subunit controls cAMP compartmentation and oncogenic signaling. *Cell* **182**, 1531–1544 e1515
44. Dumaz, N., and Marais, R. (2003) Protein kinase A blocks Raf-1 activity by stimulating 14-3-3 binding and blocking Raf-1 interaction with Ras. *J. Biol. Chem.* **278**, 29819–29823
45. Obsilova, V., and Obsil, T. (2020) The 14-3-3 proteins as important allosteric regulators of protein kinases. *Int. J. Mol. Sci.* **21**, 8824
46. Lee, S., Rauch, J., and Kolch, W. (2020) Targeting MAPK signaling in cancer: mechanisms of drug resistance and sensitivity. *Int. J. Mol. Sci.* **21**, 1102
47. Morgan, C. W., Dale, I. L., Thomas, A. P., Hunt, J., and Chin, J. W. (2021) Selective CRAF inhibition elicits transactivation. *J. Am. Chem. Soc.* **143**, 4600–4606
48. Karoulia, Z., Gavathiotis, E., and Poulikakos, P. I. (2017) New perspectives for targeting RAF kinase in human cancer. *Nat. Rev. Cancer* **17**, 676–691
49. Caunt, C. J., Sale, M. J., Smith, P. D., and Cook, S. J. (2015) MEK1 and MEK2 inhibitors and cancer therapy: the long and winding road. *Nat. Rev. Cancer* **15**, 577–592
50. Page, C. P., and Spina, D. (2011) Phosphodiesterase inhibitors in the treatment of inflammatory diseases. *Handb. Exp. Pharmacol.*, 391–414
51. Ballone, A., Centorrino, F., and Ottmann, C. (2018) 14-3-3: a case study in PPI modulation. *Molecules* **23**, 1386
52. Gigante, A., Sijbesma, E., Sanchez-Murcia, P. A., Hu, X., Bier, D., Backer, S., *et al.* (2020) A supramolecular stabilizer of the 14-3-3ζ/ERα protein-protein interaction with a synergistic mode of action. *Angew. Chem. Int. Ed. Engl.* **59**, 5284–5287
53. Ghosh, A., Ratha, B. N., Gayen, N., Mroue, K. H., Kar, R. K., Mandal, A. K., *et al.* (2015) Biophysical characterization of essential phosphorylation at the flexible C-terminal region of C-Raf with 14-3-3ζ protein. *PLoS One* **10**, e0135976
54. Gietz, R. D., and Schiestl, R. H. (2007) High-efficiency yeast transformation using the LiAc/SS carrier DNA/PEG method. *Nat. Protoc.* **2**, 31–34
55. Dar, A., Wu, D., Lee, N., Shibata, E., and Dutta, A. (2014) 14-3-3 proteins play a role in the cell cycle by shielding Cdt2 from ubiquitin-mediated degradation. *Mol. Cell. Biol.* **34**, 4049–4061
56. *Schrödinger Release 2020-4: Maestro, Force Fields, MacroModel, Prime, Protein Preparation Wizard, Ligprep, Desmond Molecular Dynamics System.* (2023). D. E. Shaw Research, New York, NY
57. Xu, Y., Ren, J., He, X., Chen, H., Wei, T., and Feng, W. (2019) YWHA/14-3-3 proteins recognize phosphorylated TFEB by a noncanonical mode for controlling TFEB cytoplasmic localization. *Autophagy* **15**, 1017–1030